Available online at www.sciencedirect.com
SCIENCE DIRECT®
Comput. Methods Appl. Mech. Engrg. 195 (2006) 3608–3621
Computer methods in applied mechanics and engineering
www.elsevier.com/locate/cma

Non-uniform grid accelerated local–global boundary condition (NG-LGBC) for acoustic scattering

Amir Boag *, Uri Shemer, Raphael Kastner

Department of Physical Electronics, School of Electrical Engineering, Tel-Aviv University, Tel-Aviv 69978, Israel

Received 1 November 2004; received in revised form 31 January 2005; accepted 22 February 2005

Abstract

A global absorbing boundary condition utilizing accelerated integration scheme based on the non-uniform grid (NG) approach is hybridized with a local boundary condition, producing an accurate and efficient mesh truncation scheme for finite method analysis of open-region acoustic scattering problems. The method affords arbitrarily shaped, in particular non-convex boundaries that conform to essentially concave obstacles of dimensions large compared with the wavelength.

Keywords: Absorbing boundary condition; Global boundary condition; Fast methods; Acoustic scattering; Kirchoff integral

1. Introduction

In solving unbounded problems by the finite element method (FEM), finite difference time domain (FDTD) or finite difference frequency domain (FDFD) methods, one often faces the need to choose between local and global absorbing boundary conditions (ABCs). Local ABCs are usually considered more efficient because they utilize a finite stencil, therefore they have become relatively popular in recent years. One can categorize two groups of local ABCs: The first group is based on local approximations of the one way wave equation or the radiation condition. Early (late 70s) local ABCs used pseudo-differential operators as generalizations of the one-way wave equations. Such ABCs were developed by Engquist and Majda [1,2]. These conditions were implemented in the context of Maxwell's equations and the Navier–Stokes equations by Mur [3], Rudy and Strikwerda [4], respectively. Bayliss and Turkel [5–8] developed an

* Corresponding author. Tel.: +972 3 6408246; fax: +972 3 6423508.
E-mail address: boag@eng.tau.ac.il (A. Boag).

0045-7825/$ - see front matter
doi:10.1016/j.cma.2005.02.028

asymptotic expansion that can be considered as a generalization of the Sommerfeld radiation condition and applied it to both time- and frequency-domain calculation. Many other local ABCs, extending the ones mentioned above, such as [9], are available in the literature. Numerically derived local ABCs have been also proposed [10]. The main drawback of these methods is in their limited accuracy and essential dependence on the angle of arrival. The second group of local ABCs overcomes this limitation by employing absorption rather than radiation-based condition. The most notable method in this class is the perfectly matched layer (PML) introduced by Berenger [11]. It appears to yield a major improvement in the reduction of boundary reflections compared to any ABC proposed previously and as such has attracted considerable attention. The PML has been formulated in terms of both Berenger's original non-Maxwellian equations and Maxwellian forms [12]. The main disadvantage of the PML is the need to surround the computational domain with a thick layer that may add a significant number of unknowns to the problem.

In addition to the aforementioned issues, a major drawback common to all local ABC formulations is the requirement for the boundary to be a convex, typically separable surface such as a box or sphere, which may not conform very well to the shape of the scattering obstacle. The convexity requirement translates into a sizeable "white space"[1] when treating an essentially concave geometry and hence implies a significant additional computational cost.

In contrast to local ABCs, global boundary conditions (GBCs) involve integration over the entire boundary of the computational domain. These formulations can be based on one of the following: (1) Kirchoff-like integration of equivalent sources on a given surface, resulting in the field on an adjacent external surface; (2) construction of an impedance-like operator (viz., a Green's function) transforming the magnetic (electric) field into the electric (magnetic) field over the surface or, equivalently, building an integral equation for a surface problem. The latter formulation is then discretized via the boundary elements method (BEM) and then incorporated as a dense block into the FEM total matrix (this procedure can be viewed as a FEM–BEM hybridization, see below). Global BCs require no approximations, thus having the potential for providing better accuracy. The boundary can trace the surface of the scattering object, avoiding the convexity requirement, thereby reducing the number of mesh points in the "white space". The main disadvantage associated with GBCs, however, is the creation of dense rather than sparse matrix blocks, rendering these methods relatively expensive in terms of computer resources. GBCs were originally developed in the early 70s in the context of the Laplace and Helmholz equations [13]. The unimoment method [15] was introduced as generalized impedance relationships in the context of individual cylindrical and spherical wave functions. The early 80s saw the global lookback scheme [14] that enabled the computational domain to be truncated near the sources. The field on the boundary was generated from those field values at retarded times on an interior surface one cell away from the boundary via an integral representation of the field. Non-local boundary conditions, in particular the Dirichlet-to-Neumann (DtN) operator [16,17], offer the advantage of being exact while allowing fast evaluation. However, these methods require a separable boundary, similarly to the unimoment method. Removal of the requirement of specific boundary shapes has been offered by the difference potential method (DPM) [18] and by the Green's function method (GFM) [19,20]. These methods provide a compromise between the efficiency and accuracy of the local and global ABCs, respectively. The GFM is the result of a purely discrete formulation of the Green's function tailored to a given arbitrary surface, rather than using an outright discretization of the continuous Green's function. Extensive survey of the ABC literature can be found in [21–23].

Hybridization methods for GBCs in the context of the FEM–BEM, referred to as the FEM-boundary integral (FEM-BI) approach, are reviewed in [24, Chapters 13.3 and 13.4]. This hybridization scheme possesses the drawbacks in terms of computational cost mentioned above in the context of GBCs, unless an

[1] The "white space" is the free space region between the scatterer and the ABC, needed for application of finite methods, however containing information that depends on the solution within the scatterer itself and in this sense may be considered redundant.

efficient integration method is employed. In order to improve efficiency, discretized integration can be performed by using the fast multipole method (FMM) [25–28]. This method is known to reduce the computational complexity of each multiplication operation from $\mathcal{O}(N^2)$ to $\mathcal{O}(N^{1.5})$, where N is proportional to the number of boundary unknowns. Multilevel fast multipole algorithm (MLFMA) can further reduce computational complexity to $\mathcal{O}(N \log N)$ [29–34]. An alternative fast GBC method, proposed in [35], employs a two level non-uniform grid (NG) algorithm [36] for accelerating the pertinent surface integrations.

For any GBC, artificial resonances resulting from the closed surface integral formulation, may result in a high condition number for the FEM matrix, which in turns causes iterative solution algorithms to slow down or stagnate at times. In particular, if the closed surface has concave portions, that are of primary interest here, additional resonance artifacts may occur due to internal reflections within the concave inlet.

Blending local and global ABCs is a remedy to the aforementioned difficulty. Recently suggested novel GBCs combining the local–global blend with fast integration algorithms are the FEM/adaptive absorbing boundary condition method [37] and its time-domain counterpart using the plane wave time domain (PWTD) method [38].

In this work, it is proposed to alleviate the aforementioned problems by hybridizing the fast scheme of [35] with a conventional local ABC, such as Mur's in order to achieve enhanced accuracy and improved convergence for problems of the concave type as defined in Section 2. The hybridization scheme, first proposed in [39], is introduced in Section 3. The details of the fast integration scheme are reviewed in Section 4, and numerical tests in Section 5 show that this algorithm is indeed capable of reducing the computational cost of evaluating the boundary integrals from $\mathcal{O}(N^2)$ to $\mathcal{O}(N^{1.5})$. A multilevel NG algorithm, to be developed in the next phase of this work, will achieve an asymptotic complexity of $\mathcal{O}(N \log N)$. Improved convergence rate of the iterative algorithm, thanks to the proposed hybridization of the boundary conditions, is also demonstrated in Section 5. Conclusions are duly drawn in Section 6.

2. Problem specification

Consider a two-dimensional (2D) problem of acoustic scattering by an arbitrary shaped obstacle surrounded by an unbounded, ideal, compressible and homogeneous medium characterized by the sound propagation velocity c. The problem is characterized by the geometry and the incident field being uniform along the z-axis. In the x–y-plane, the scatterer can be circumscribed by a circle of radius R. Let the body be immersed in an incident wave defined by acoustic pressure $P^{\text{inc}}(\mathbf{r})$ with harmonic time dependence $e^{\jmath\omega t}$ assumed and suppressed ($\jmath = \sqrt{-1}$). Our objective is to determine the field scattered by the obstacle, $P(\mathbf{r}) = P^{\text{tot}}(\mathbf{r}) - P^{\text{inc}}(\mathbf{r})$, whereas $P^{\text{tot}}(\mathbf{r})$ denotes the total field in the presence of the obstacle. Within the medium surrounding the obstacle, each of the three time harmonic constituents $P(\mathbf{r})$, $P^{\text{tot}}(\mathbf{r})$, and $P^{\text{inc}}(\mathbf{r})$ obeys the Helmholtz equation $(\nabla^2 + k^2)P = 0$, where $k = \omega/c$ is the intrinsic wave number. The scattered field $P(\mathbf{r})$ also satisfies the Sommerfeld radiation condition $\lim_{r\to\infty}\sqrt{r}(\partial_r + \jmath k)P = 0$.

Towards solving the problem, we consider the scattered field discretized via a finite difference frequency domain (FDFD) or an FEM formulation. Enclosing the obstacle within a closed convex boundary $\Gamma_{\text{o}}^{\text{convex}}$ (see Fig. 1(a)), one may apply a number of discretized local ABCs on this boundary, all of which take the following general form

$$\sum_{i=1}^{M} a_i P(\mathbf{r}_i) = 0, \tag{1}$$

where a_i are constant coefficients characteristic of a particular ABC. For the sake of simplicity, we consider a local point numbering where M is the number of points within the ABC stencil. As an example, for the Mur ABC on a Cartesian finite difference mesh, we have $M = 6$ where the sampling points reside on a dou-

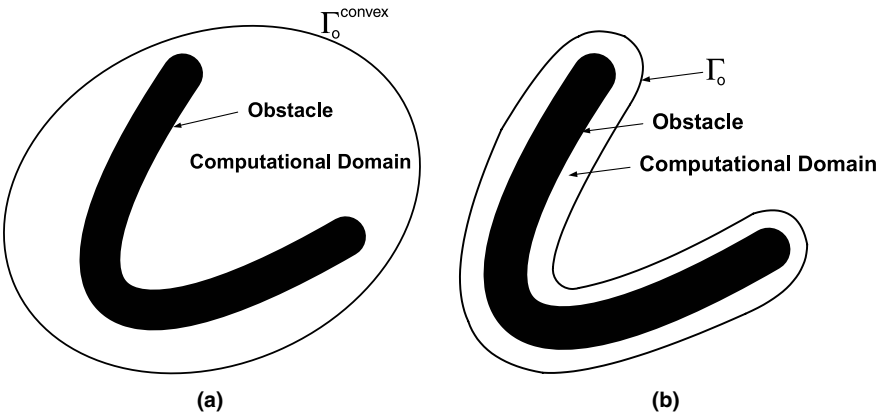

Fig. 1. A general, non-convex obstacle in: (a) a convex computational domain and (b) a conformal computational domain.

ble-layered boundary Γ_o as shown in Fig. 2. The numerical size of the problem is characterized by $N = kR$ that serves as a large parameter in evaluating the asymptotic computational complexity. For the discretized domain within the convex boundary, the number of unknowns is of $\mathcal{O}(N^2)$. In the context of this work, we concentrate on essentially concave bodies, such as the thin shell type of obstacle depicted in Fig. 1(a). When such a obstacle is embedded in a convex computational domain it creates a relatively large "white space" formed between the obstacle and the boundary, including the concave inlet. In this case, the majority of the unknowns are needed to mesh the "white space". When solving the problem iteratively, such formulation would require $\mathcal{O}(N^2)$ operations per iteration. In contrast, for the same structure, the number of unknowns on its surface is of $\mathcal{O}(N)$. Thus, it appears tempting to deform the Γ_o^{convex} to be conformal with the obstacle. This new boundary, designated Γ_o (see Fig. 1(b)) is assumed to follow the obstacle surface at a fixed distance (in terms of wavelength and independent of N). The total number of unknowns is then reduced from $\mathcal{O}(N^2)$ to $\mathcal{O}(N)$ at the expense of making the outer boundary non-convex, thus prohibiting the usage of local ABCs. Numerically efficient extension of (1) to concave boundaries forms the subject of this work.

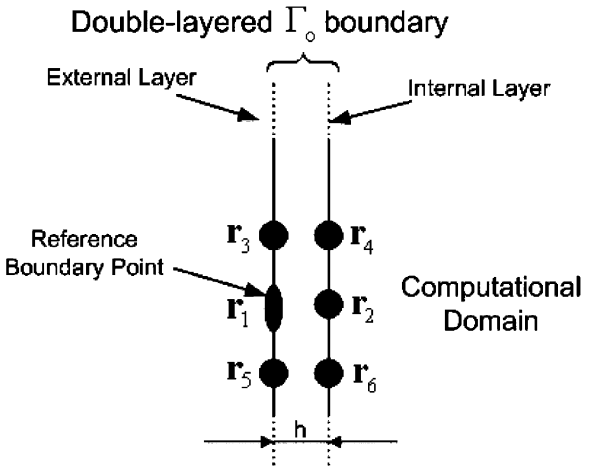

Fig. 2. Six-point stencil of Mur ABC on a double layered boundary.

3. Local–global boundary condition (LGBC)

Extension of Eq. (1) to concave boundaries requires the introduction of a boundary integral type correction factor. Let $\widehat{P}(\mathbf{r}_i)$ denote the scattered acoustic field at a point on Γ_o, as calculated using a Kirchoff type integral

$$\widehat{P}(\mathbf{r}_i) = \oint_{\Gamma_s} \left[P(\mathbf{r}') \frac{\partial G(\mathbf{r}_i, \mathbf{r}')}{\partial n'} - G(\mathbf{r}_i, \mathbf{r}') \frac{\partial P(\mathbf{r}')}{\partial n'} \right] \mathrm{d}s', \tag{2}$$

where Γ_s is an arbitrarily shaped closed contour between the obstacle and Γ_o, and $G(\mathbf{r}, \mathbf{r}') = \frac{1}{4j} \mathrm{H}_0^{(2)}(k|\mathbf{r} - \mathbf{r}'|)$ is the 2D Green function, $\mathrm{H}_0^{(2)}(\cdot)$ being the Hankel function of second kind and order 0. By analogy with [38], we propose a general hybrid boundary condition

$$\sum_{i=1}^{M} a_i [P(\mathbf{r}_i) - \widehat{P}(\mathbf{r}_i)] = 0. \tag{3}$$

Eq. (3) is readily satisfied for a convex Γ_o since both $P(\mathbf{r}_i)$ and $\widehat{P}(\mathbf{r}_i)$ should individually satisfy the local ABC (1), i.e., $\sum_{i=1}^{M} a_i P(\mathbf{r}_i) = 0$ and $\sum_{i=1}^{M} a_i \widehat{P}(\mathbf{r}_i) = 0$, thus reducing (3) to a trivial subtraction of zeros. In general cases that include concave portions of Γ_o, we should have $P(\mathbf{r}_i) = \widehat{P}(\mathbf{r}_i)$ by virtue of the Radiation Integral formulation as in [35]. Alternatively, this local–global boundary condition (LGBC) may be viewed as a preconditioning operation performed on the formulation in [35] by means of a linear combination between the generalized local ABC in (1) and the radiation integral formulation $P(\mathbf{r}_i) = \widehat{P}(\mathbf{r}_i)$ (see numerical results showing improved convergence of the proposed scheme in Section 5).

In summary, the LGBC (3) is applicable to arbitrarily shaped boundaries, provided that the numerical evaluation of the radiation integral in (2) is done in an economically viable fashion, as proposed in the following section.

4. Non-uniform grid (NG) approach

In this section, we show that the computational complexity of evaluating the scattered acoustic field $\widehat{P}(\mathbf{r}_i)$ can be reduced below the $\mathcal{O}(N^2)$ cost of the straightforward computation via (2). The integral (2) can be decomposed into distinct near-field and far-field contributions. To this end, we divide Γ_s into Q disjoint subdomains of roughly equal size, $\Gamma_s = \bigcup_{q=1}^{Q} \overline{\Gamma}_q$. The smallest circle circumscribing each subdomain $\overline{\Gamma}_q$ has a radius $\overline{R}_q$ and is centered at $\bar{\mathbf{r}}_q$ (this circle may or may not intercept Γ_o or the obstacle). Based on this division, the scattered acoustic field at the observation point $\mathbf{r}_i$ is computed as an aggregation of partial fields, i.e.,

$$\widehat{P}(\mathbf{r}_i) = \sum_{q=1}^{Q} \overline{P}_q(\mathbf{r}_i), \tag{4}$$

where $\overline{P}_q(\mathbf{r}_i)$ denotes the partial acoustic field due to the restriction of the integral to subdomain $\overline{\Gamma}_q$. The partial field $\overline{P}_q(\mathbf{r}_i)$ is evaluated in a way dependent on the distance $\rho_q(\mathbf{r}_i) = |\mathbf{r}_i - \bar{\mathbf{r}}_q|$. Relatively small and large such distances define the near and far field zones, respectively, characterized by different integration rules. The near field zone is defined by $\rho_q(\mathbf{r}_i) < \Omega_R \overline{R}_q$, where $\Omega_R > 1$ is a parameter determining the near zone radius relative to that of the source subdomain $\overline{\Gamma}_q$. In this zone, $\overline{P}_q(\mathbf{r}_i)$ is computed via a straightforward integration as follows:

$$\overline{P}_q(\mathbf{r}_i) = \int_{\overline{\Gamma}_q} \left[P(\mathbf{r}') \frac{\partial G(\mathbf{r}_i, \mathbf{r}')}{\partial n'} - G(\mathbf{r}_i, \mathbf{r}') \frac{\partial P(\mathbf{r}')}{\partial n'} \right] \mathrm{d}s'; \quad \rho_q(\mathbf{r}_i) < \Omega_R \overline{R}_q. \tag{5}$$

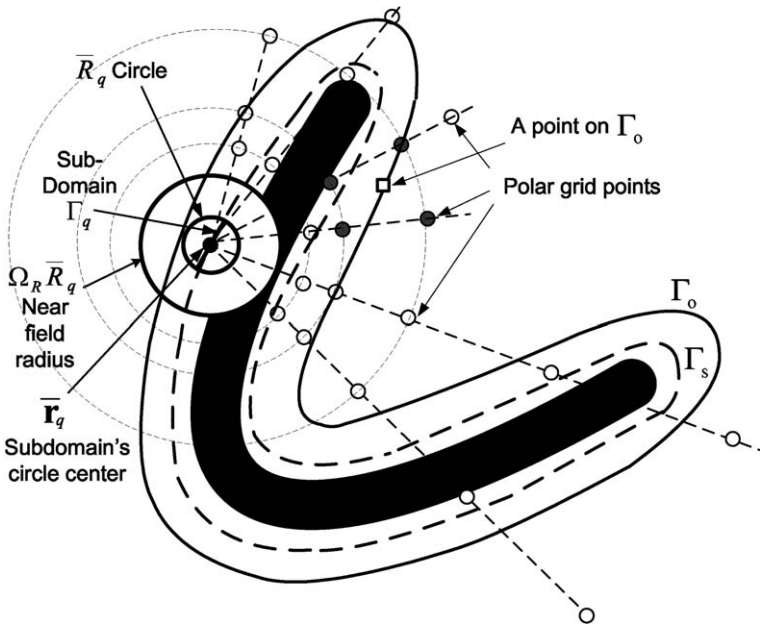

Fig. 3. A portion of the non-uniform polar grid (NG) for a selected subdomain and four NG points (shown as solid circles) used in the bilinear interpolation for a particular point on Γ_o.

In the far field zone of $\overline{\Gamma}_q$ ($\rho_q(\mathbf{r}_i) \geqslant \Omega_R \overline{R}_q$), we modify the calculation as follows. First, we compute the *phase and amplitude compensated* partial field $\widetilde{P}_q$ defined as

$$\widetilde{P}_q(\tilde{\mathbf{r}}_n^q) = \sqrt{\tilde{\rho}_q(\tilde{\mathbf{r}}_n^q)}\mathrm{e}^{+jk\tilde{\rho}_q(\tilde{\mathbf{r}}_n^q)} \int_{\overline{\Gamma}_q} \left[P(\mathbf{r}') \frac{\partial G(\tilde{\mathbf{r}}_n^q, \mathbf{r}')}{\partial n'} - G(\tilde{\mathbf{r}}_n^q, \mathbf{r}') \frac{\partial P(\mathbf{r}')}{\partial n'} \right] \mathrm{d}s', \quad \rho_q(\tilde{\mathbf{r}}_n^q) \geqslant \Omega_R \overline{R}_q, \tag{6}$$

where $\{\tilde{\mathbf{r}}_n^q\}_{n=1}^{\overline{N}_q}$ is a set of observation points in the vicinity the contour Γ_o comprising a polar Non-uniform grid (NG) whose center is at $\bar{\mathbf{r}}_q$ (see Fig. 3)[2] and $\tilde{\rho}_q(\mathbf{r}) = \sqrt{(\rho_q(\mathbf{r}))^2 + \overline{R}_q^2/2}$. The factor $\sqrt{\tilde{\rho}_q(\tilde{\mathbf{r}}_n^q)}\mathrm{e}^{+jk\tilde{\rho}_q(\tilde{\mathbf{r}}_n^q)}$ is designed to approximately offset the rapid oscillations and amplitude drop-off typical of the large argument asymptotic behavior of the Hankel functions appearing both in the Green's function and its derivative. The compensation makes $\widetilde{P}_q(\cdot)$ in (6) smooth on a scale well beyond the wavelength, thereby allowing the NG to be very sparse, containing only $\overline{N}_q = \mathcal{O}(N^{1/2})$ points per subdomain, as shown below. Subsequently, the samples over the NG, $\widetilde{P}_q(\tilde{\mathbf{r}}_n^q)$, are employed to obtain the field values at the desired points $\mathbf{r}_i$ on Γ_o by a local interpolation

$$\widetilde{P}_q(\mathbf{r}_i) = \sum_{n:\ \tilde{\mathbf{r}}_n^q \in \sigma(\mathbf{r}_i)} w_n^q(\mathbf{r}_i) \widetilde{P}_q(\tilde{\mathbf{r}}_n^q); \quad \rho_q(\mathbf{r}_i) \geqslant \Omega_R \overline{R}_q, \tag{7}$$

where $w_n^q(\mathbf{r}_i)$ denote the interpolation weights and $\sigma(\mathbf{r}_i)$ is the neighborhood of $\mathbf{r}_i$ containing the grid points $\tilde{\mathbf{r}}_n^q$ needed for interpolation at $\mathbf{r}_i$. As an example, for bilinear interpolation, $\sigma(\mathbf{r}_i)$ contains four grid points and the interpolation weights are obtained as products of the conventional linear interpolation coefficients. The interpolation (7) is then followed by phase and amplitude restoration

[2] Both subscripts n and i denote observation points, however $\{\mathbf{r}_i\} \in \Gamma_o$, while $\{\tilde{\mathbf{r}}_n^q\} \in$ NG centered about $\bar{\mathbf{r}}_q$.

$$\overline{P}_q(\mathbf{r}_i) = \frac{\mathrm{e}^{-jk\tilde{\rho}_q(\mathbf{r}_i)}}{\sqrt{\tilde{\rho}_q(\mathbf{r}_i)}}\widetilde{P}_q(\mathbf{r}_i); \quad \rho_q(\mathbf{r}_i) \geqslant \Omega_{\mathrm{R}}\overline{R}_q. \tag{8}$$

Finally, the total field is obtained by aggregating all the partial ones via (4).

Note that the combined computational cost of the local interpolation (7) and the phase/amplitude restoration (8) is substantially lower than that of direct computation via (2). Significant computational savings are thus achieved since the partial fields in (6) are computed over a coarse sampling grid in the vicinity of Γ_{o}.

With the goal of designing an optimal NG, $\{\tilde{\mathbf{r}}_n^q\}_{n=1}^{\overline{N}_q}$, it is advantageous to consider the partial field $\widetilde{P}_q(\rho_q, \phi_q)$ as a function of the polar coordinates ρ_q and ϕ_q of the local coordinate system centered about $\bar{\mathbf{r}}_q$. We show that the angular and radial sampling rate requirements are substantially different, making this distinction very important. In order to determine the minimal sampling rates for $\widetilde{P}_q(\rho_q, \phi_q)$ versus both ρ_q and ϕ_q, we can approximate the phase and amplitude compensated field in (6) using large argument asymptotic expressions for the Hankel functions:

$$\widetilde{P}_q(\mathbf{r}) \sim \int_{\overline{\Gamma}_q} A(\mathbf{r}, \mathbf{r}')\mathrm{e}^{\jmath k(\tilde{\rho}_q(\mathbf{r})-\rho))}\,\mathrm{d}s', \tag{9}$$

where $\rho = |\mathbf{r} - \mathbf{r}'|$ and

$$A(\mathbf{r}, \mathbf{r}') = \sqrt{\frac{\jmath\tilde{\rho}_q}{8\pi k\rho}}\left[k(\hat{\boldsymbol{\rho}}\cdot\hat{\mathbf{n}}')P(\mathbf{r}') - \frac{1}{\jmath}\frac{\partial P(\mathbf{r}')}{\partial n'}\right] \tag{10}$$

with $\hat{\boldsymbol{\rho}} = (\mathbf{r} - \mathbf{r}')/\rho$. The function $A(\mathbf{r},\mathbf{r}')$ varies slowly with respect to the observation point $\mathbf{r}$ ($\mathbf{r} - \bar{\mathbf{r}}_q = (\rho_q, \phi_q)$). Thus, we can approximately consider the integral (9) as a superposition of the following exponential terms

$$\mathrm{e}^{\jmath k(\tilde{\rho}_q(\mathbf{r})-\rho)} \approx \mathrm{e}^{jk\left(\frac{\overline{R}_q^2}{4\rho_q} - \frac{\rho_q'^2}{2\rho_q}(1-\cos^2(\phi_q-\phi_q'))+\rho_q'\cos(\phi_q-\phi_q')\right)}, \quad \rho_q \gg \overline{R}_q, \tag{11}$$

where $(\rho_q', \phi_q') = \mathbf{r}' - \bar{\mathbf{r}}_q$ are the source point polar coordinates in the $\bar{\mathbf{r}}_q$ centered coordinate system. With respect to angular dependence, the main variation comes from the $\mathrm{e}^{\jmath k\rho_q'\cos(\phi_q-\phi_q')}$ term, that can be represented by the Jacobi–Anger expansion:

$$\mathrm{e}^{\jmath k\rho_q'\cos(\phi_q-\phi_q')} = J_0(k\rho_q') + 2\sum_{n=1}^{\infty}\jmath^n J_n(k\rho_q')\cos[n(\phi_q - \phi_q')], \tag{12}$$

where $J_n(\cdot)$ denotes the Bessel function of order n. Since Bessel functions decay faster than exponentially for orders higher than the argument, and the argument in (12) is bounded by $k\rho_q' \leqslant k\overline{R}_q$, the series (12) can be truncated uniformly for all source points within the subdomain under consideration, so that $\widetilde{P}_q(\rho_q, \phi_q)$ is an essentially bandlimited function of ϕ_q. Consequently, the sampling rate in ϕ_q should satisfy the criterion $f_\phi^{\mathrm{s}} = \Omega_\phi k\overline{R}_q/\pi$, where $\Omega_\phi > 1$ is the angular oversampling ratio.

In terms of radial dependence on ρ_q, the integral (9) comprises a superposition of exponential terms of the type $\exp[\jmath\omega_\alpha\alpha]$, where we define a new reciprocal radial variable $\alpha \doteq 1/\rho_q$ and $\omega_\alpha = k(\frac{\overline{R}_q^2}{4} - \frac{\rho_q'^2}{2}(1-\cos^2(\phi_q - \phi_q')))$. For a source point $\mathbf{r}'$ within the qth subdomain (circumscribed by a circle of radius $\overline{R}_q$), the frequency ω_α is bounded, namely, $|\omega_\alpha| \leqslant k\overline{R}_q^2/4$. The α-sampling rate f_α^{s} should satisfy $f_\alpha^{\mathrm{s}} = \Omega_\rho \max|\omega_\alpha|/\pi = \Omega_\rho k\overline{R}_q^2/4\pi$, where $\Omega_\rho > 1$ is the radial oversampling ratio. A uniform sampling versus α is employed in the far field of the qth subdomain, namely for $\Omega_{\mathrm{R}}\overline{R}_q \leqslant \rho_q < 2R$ or $\alpha \in ((2R)^{-1}, (\Omega_{\mathrm{R}}\overline{R}_q)^{-1}]$. This translates into a highly non-uniform sampling grid versus ρ_q, to which we refer hitherto as the non-uniform grid (NG).

Next, we show that, as a consequence of the above observations, the number $\overline{N}_q$ of non-redundant samples of the scattered field on the NG, $\{\widetilde{P}_q(\tilde{\mathbf{r}}_n^q)\}_{n=1}^{\overline{N}_q}$, $\tilde{\mathbf{r}}_n^q = (\tilde{\rho}_n^q, \tilde{\phi}_n^q)$, that needs to be computed is proportional to the subdomain size. Note that the NG is constructed in the (ρ_q, ϕ_q) coordinate system according to the above sampling criteria and comprises the minimum number of points that allows interpolation of a prescribed order to all points on the surface Γ_o. For example, for a bi-linear interpolation, every point on Γ_o should be located within a polar grid quadrilateral cell with NG grid points serving as it vertices as shown in Fig. 3. Higher order interpolation schemes would require a thicker layer of sample points in the vicinity of Γ_o. In order to make an estimate of the number of the NG points, we have to assume that Γ_o is sufficiently well behaved in the following sense: If Γ_o is represented in terms of a parameter s in the form $(\rho_q^\Gamma(s), \phi_q^\Gamma(s))$, we assume that the number of extrema of $\rho_q^\Gamma(s)$ and $\phi_q^\Gamma(s)$ is uniformly bounded for all subdomains. This requirement can be somewhat relaxed since excursions of Γ_o smaller than the interpolation cell size are not significant. We will not dwell in this context on the precise minimum requirements on Γ_o. Specifically, assume that the part of Γ_o external to the near-field circle comprises N_e segments, each one bounded by extrema of either $\rho_q^\Gamma(s)$ or $\phi_q^\Gamma(s)$. Let the ith segment be bounded by the extrema $(\rho_{i,1}^e, \phi_{i,1}^e)$ and $(\rho_{i,2}^e, \phi_{i,2}^e)$. Then, a bound on the number of coarse grid points $\overline{N}_q$ can be expressed as

$$\overline{N}_q \leqslant \sum_{i=1}^{N_e} (C_\phi^s |f_\phi^s(\phi_{i,2}^e - \phi_{i,1}^e)| + C_\rho^s |f_\alpha^s[(\rho_{i,2}^e)^{-1} - (\rho_{i,1}^e)^{-1}]| + C^s), \tag{13}$$

where C_ϕ^s, C_ρ^s, and C^s are positive constants. Since $\forall i$, $\rho_i^e > \Omega_R \overline{R}_q$, and using the fact that $\phi_{i,2}^e - \phi_{i,1}^e \leqslant 2\pi$, we have

$$\overline{N}_q \leqslant k\overline{R}_q N_e \left(2C_\phi^s \Omega_\phi + \frac{C_\rho^s \Omega_\rho}{4\pi\Omega_R}\right) + C^s N_e. \tag{14}$$

In order to estimate the computational cost of evaluating the acoustic field $\widehat{P}(\mathbf{r}_i)$ for all points on Γ_o, we assume that all subdomains are approximately equal in size, i.e., $\forall q\ \overline{R}_q \approx \overline{R}$, which allows us to henceforth replace the individual notations $\overline{N}_q$ by the common notation $\overline{N}$ to designate the number of NG points per any subdomain. In (6), $\widetilde{P}_q(\tilde{\rho}_q^n, \tilde{\phi}_q^n)$ is evaluated at $\mathcal{O}(\overline{N})$ points at a cost of $c_1\overline{N}^2$, where $\overline{N} = \mathcal{O}(k\overline{R})$, and, subsequently, interpolated to $\mathcal{O}(N)$ points at a cost of $c_2 N$, c_1 and c_2 being constants. Near field computations for each subdomain via (4) also requires $\mathcal{O}(\overline{N}^2)$ operations. The number of subdomains Q for reasonably behaved surfaces is roughly proportional to the ratio $N/\overline{N}$. Thus, the computational burden of computing and aggregating Q partial fields amounts to

$$C \propto \frac{N}{\overline{N}}(c_1'\overline{N}^2 + c_2 N), \tag{15}$$

where the term $c_1'\overline{N}^2$ accounts for both coarse grid and near field computations. One finds from (15) that the lowest asymptotic complexity of $\mathcal{O}(N^{1.5})$ is attained for $\overline{N} = c_3\sqrt{N}$, $c_3 = \sqrt{c_2/c_1'}$. This result compares favorably with the $\mathcal{O}(N^2)$ cost of the straightforward evaluation of (2). The complexity estimate obtained herein is thus similar to that of the two-level fast multipole method (FMM) [27].

5. Numerical results

A computer code implementing the NG accelerated LGBC described in the previous sections has been developed for the second order accurate, central-difference discretization of the Helmholtz equation. A numerical implementation of the NG algorithm involves making choices regarding the interpolation, selection of the quadrature rule, and the amount of oversampling. Also, the spacing between the LGBC contours Γ_o and Γ_s and the scatteres and shapes of these contours should be selected. All of these parameters

are interrelated and they affect the accuracy as well as the complexity of the algorithm. While a comprehensive study of the optimal parameter selection is beyond the scope of this paper, we present some choices facilitating easy implementation as adopted in our code to demonstrate the numerical performance of the proposed algorithm.

As a representative example of a non-convex obstacle, we study a thin rectangular L-shaped obstacle depicted in Fig. 4 with dimensions $W = L = 4\lambda$ where $\lambda = 2\pi/k$ is the wavelength in the surrounding medium. We assume perfectly soft boundary condition $P^{\text{tot}} = 0$ on the obstacle surface, such that the scattered acoustic field on the obstacle surface is given by $P = -P^{\text{inc}}$. The excitation is provided by a plane wave propagating in the positive x-direction, i.e., $P^{\text{inc}} = \mathrm{e}^{-\jmath kx}$.

For the NG-LGBC scheme, the issue of interpolation deserves the most attention when implementing the NG approach. Clearly, there are numerous ways to perform interpolation and the selection of the optimal one may not be trivial. In our code, only linear interpolation for both α_q and ϕ_q is implemented, for the sake of simplicity. The contours Γ_{o} and Γ_{s} are piecewise rectangular, conforming with the obstacle as shown in Fig. 4(b). The finite difference mesh size is set to $h = \lambda/40$. The outer boundary Γ_{o} comprises, in fact, two layers as shown in Fig. 2, spaced one mesh size h apart. The spacings between Γ_{s} and the obstacle, and between Γ_{s} and Γ_{o} are $\lambda/2$ and λ, respectively. Note that the piecewise rectangular shape of Γ_{s} is natural for the finite difference formulation, though it is expected to somewhat harm the accuracy of the integration.

The numerical study involves the issues of accuracy and numerical efficiency of the proposed algorithm. We compare the accuracy of the NG-LGBC solution with that obtained by the LGBC with direct numerical integration of Eq. (2), both cases using the conformal computational domain shown in Fig. 4(b). We tune the accuracy of the NG evaluation by selecting the oversampling parameter $\Omega = \Omega_\rho = \Omega_\phi$. The NG evaluation error is defined as a difference between the result of the NG scheme and that of the direct integration of Eq. (2) using the same quadrature rule and other parameters. The maximum and root mean square (RMS) values of the NG error over the entire boundary Γ_{o} for a typical source field on Γ_{s} serve as reliable estimates of the NG accuracy. To this end, Fig. 5 presents the normalized maximum and RMS errors over Γ_{o} versus Ω with the near field region defined as $\Omega_{\text{R}} = 3$. The results demonstrate the quadratic convergence of the method (as expected) for linear interpolation. In applying the NG algorithm to the example below, we set the oversampling factor at $\Omega = 8$.

The aforementioned sampling rate results in $N_{\text{o}} = 2440$ points along Γ_{o}. Plots of the amplitude and phase of the total acoustic field computed using the NG accelerated and direct integration LGBC algo-

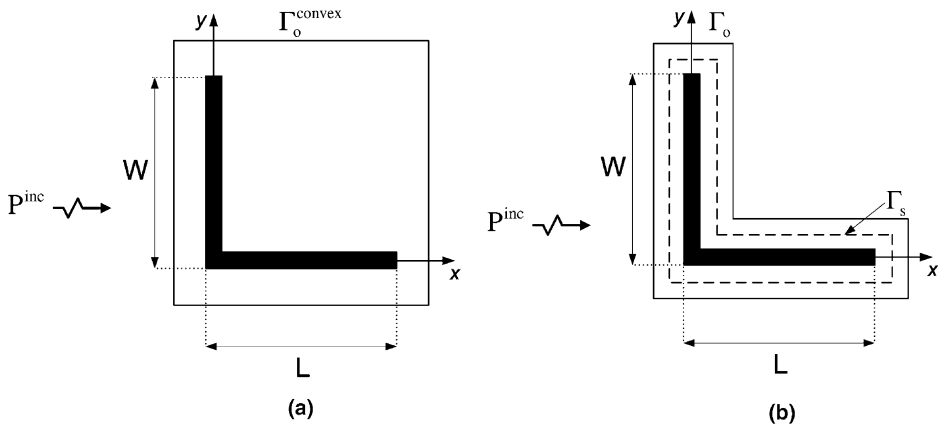

Fig. 4. L-shaped obstacle enclosed in: (a) convex computational domain, (b) conformal computational domain.

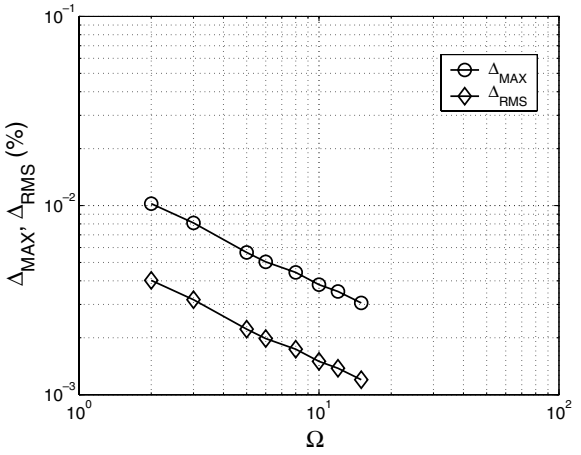

Fig. 5. Normalized maximum and RMS errors on Γ_o versus oversampling factor Ω.

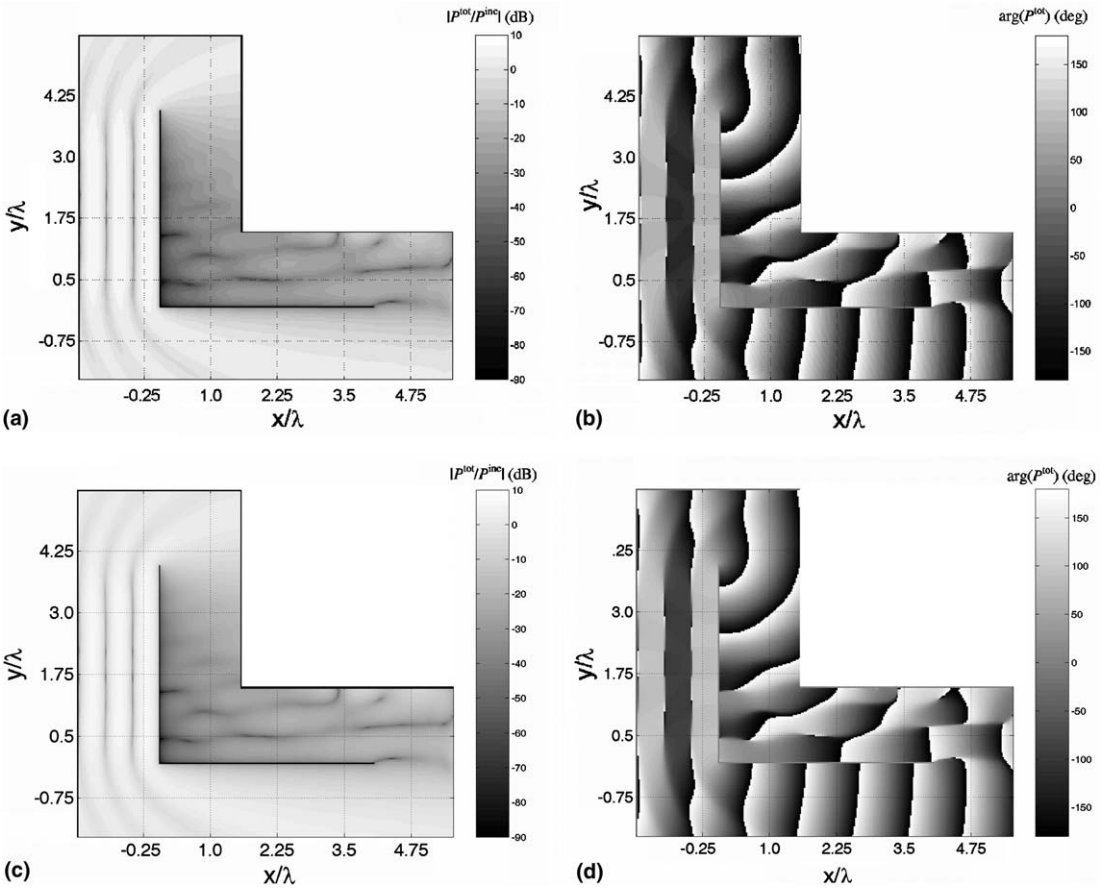

Fig. 6. Total acoustic pressure computed using LGBC via (I) direct integration: (a) amplitude; (b) phase, and (II) NG: (c) amplitude; (d) phase.

rithms, both on the conformal computational domain of Fig. 4(b) are shown in Fig. 6. Both results visibly coincide for amplitude as well as phase. In order to examine the fields in more detail, Fig. 7(a)–(d) present the x- and y-cuts of the results. Clearly, the accuracy is very good in both the lit and shadow regions.

The computational complexity is assessed by considering obstacles of various sizes, obtained by scaling the dimensions of the obstacle of Fig. 4 (or alternatively, the frequency). Note that the spacings between Γ_s and the obstacle, and between Γ_s and Γ_o remain $\lambda/2$ and λ, respectively. The computational cost of a single iteration (in FLOPS) versus the number of points on Γ_o is depicted in Fig. 8 for three implementations as

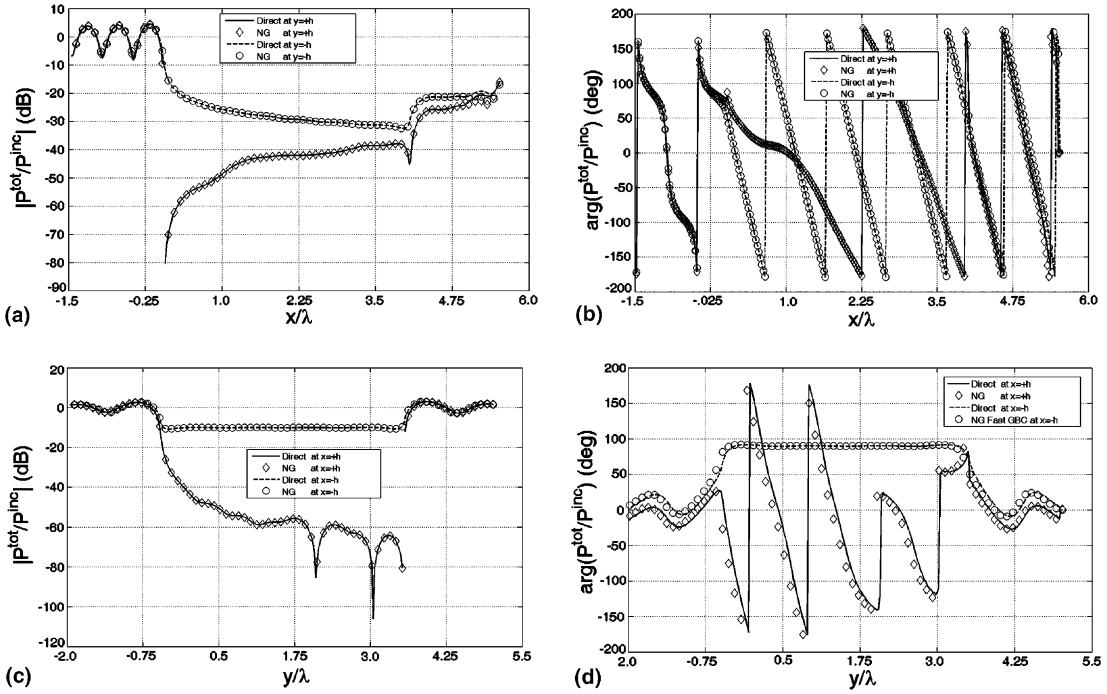

Fig. 7. Total acoustic pressure computed using direct and NG integrations LGBC: (a) amplitude versus x; (b) phase versus x; (c) amplitude versus y; (d) phase versus y.

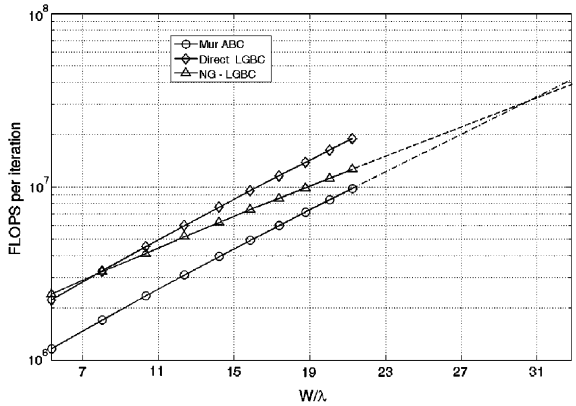

Fig. 8. Computational cost of various boundary conditions versus obstacle size in wavelengths.

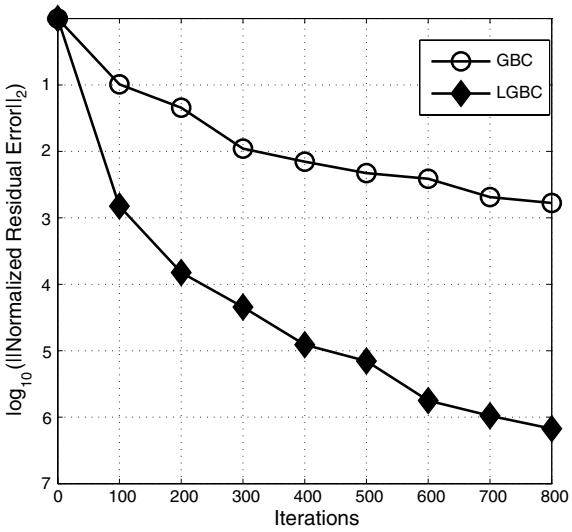

Fig. 9. Convergence rates of the GMRES algorithm for the LGBC in comparison to a GBC with Kirchoff-like integration of equivalent sources on Γ_s, resulting in the field on Γ_o.

follows: (i) the conventional Mur ABC on the boundary Γ_o^{convex} of a rectangular computational domain shown Fig. 4(a) where the spacing between Γ_o^{convex} and the obstacle is set at 1.5λ, producing a $7\lambda \times 7\lambda$ large computational domain; (ii) the LGBC with a straightforward implementation of Eq. (2) and (iii) the NG accelerated LGBC algorithm. The number of subdomains is duly scaled with the obstacle size (or equivalently, with k), that is, $Q \propto N^{0.5}$ in accordance with the development around (15). The slopes of both the direct computation and the six-point Mur boundary condition are in line with the expected $\mathcal{O}(N^2)$ behavior. The trend of the NG-LGBC algorithm, as observed in this curve, validates the estimated complexity of $\mathcal{O}(N^{1.5})$ for the NG algorithm. Extrapolation of these three curves leads to the conclusion that the NG-LGBC algorithm with the two-level domain decomposition scheme becomes more attractive for obstacle dimensions of $W = L \approx 30\lambda$ and beyond.

As mentioned above, the LGBC is also designed to reduce the condition number in comparison with existing GBCs. It thus serves as a preconditioner in the GMRES algorithm used for solving the matrix equation. Indeed, Fig. 9 shows that convergence of the LGBC is faster than that of a GBC that utilizes Kirchoff-like integration (2) to compute fields at points on the outer boundary.

6. Conclusions

A novel fast iterative algorithm based on a hybrid boundary integral formulation, coupled with a non-uniform polar grid (NG) scheme has the potential of overcoming some of the limitations of local ABC schemes. The algorithm applies to scattering problems with arbitrary shaped exterior boundaries and allows for a significant reduction in the size of the "white space" in cases characterized by essentially concave geometries. In our numerical example we considered a thin shell obstacle although arbitrarily shaped inhomogeneous obstacle can be treated the same way. An efficient and accurate multidimensional interpolation scheme is a key to the implementation of the method. A multilevel NG algorithm will attain an asymptotic complexity of $\mathcal{O}(N \log N)$.

Acknowledgments

A. Boag acknowledges partial support by the Israel Science Foundation under Grant No. 224/03. R. Kastner acknowledges partial support by the US–Israel Bi-National Science Foundation under Grant No. 1999420.

References

[1] B. Engquist, A. Majda, Absorbing boundary conditions for the numerical simulation of waves, Math. Comput. 31 (1977) 629–651.
[2] B. Engquist, A. Majda, Radiation boundary conditions for acoustic and elastic wave calculations, Commun. Pure Appl. Math. 32 (1979) 313–357.
[3] G. Mur, Absorbing boundary conditions for the finite-difference approximation of the time-domain electromagnetic-field equations, IEEE Trans. Electromagn. Compat. EMC-23 (1981) 377–382.
[4] D. Rudy, J. Strikwerda, A non-reflecting outflow boundary condition for subsonic Navier–Stokes calculations, J. Comput. Phys. 36 (1980) 55–70.
[5] A. Bayliss, E. Turkel, Radiation boundary conditions for wave-like equations, Commun. Pure Appl. Math. 33 (1980) 707–725.
[6] A. Bayliss, E. Turkel, Outflow boundary conditions for fluid dynamics, SIAM J. Sci. Stat. Comput. 3 (1982) 250–259.
[7] A. Bayliss, E. Turkel, Far-field boundary conditions for compressible flows, J. Comput. Phys. 48 (1982) 182–199.
[8] A. Bayliss, M. Gunzburger, E. Turkel, Boundary conditions for numerical solution elliptic equations in exterior domains, SIAM J. Appl. Math. 42 (1982) 430–451.
[9] R.L. Higdon, Numerical absorbing boundary conditions for the wave equation, Math. Comput. 49 (1987) 65–90.
[10] A. Boag, A. Boag, R. Mittra, A numerical absorbing boundary condition for edge-based finite element analysis, Microwave Opt. Technol. Lett. 7 (16) (1994) 733–737.
[11] J.P. Berenger, A perfectly matched layer for the absorption of electromagnetics waves, J. Comput. Phys. 114 (1) (1994) 185–200.
[12] R.W. Ziolkowski, Maxwellian material based absorbing boundary conditions, Comput. Methods Appl. Mech. Engrg. 169 (1999) 237–262.
[13] B.H. McDonald, A. Wexler, Finite-element solution of unbounded field problems, IEEE Trans. Microwave Theory Tech. MTT-20 (1972) 841.
[14] R.W. Ziolkowski, N.K. Madsen, R.C. Carpenter, Three-dimensional computer modeling of electromagnetic fields: a global lookback lattice truncation scheme, J. Comput. Phys. 50 (1983) 360–408.
[15] K.K. Mei, Unimoment method of solving antenna and scattering problems, IEEE Trans Antennas Propagat. 22 (1974) 760–766.
[16] D. Givoli, J.B. Keller, A finite element method for large domains, Comput. Methods Appl. Mech. Engrg. 76 (1989) 41–66.
[17] D. Givoli, J.B. Keller, Non-reflecting boundary conditions for elastic waves, Wave Motion 12 (1990) 261–279.
[18] V.S. Ryaben'kii, S.V. Tsynkov, Artificial boundary conditions for the numerical solution of external viscous flow problems, SIAM J. Numer. Anal. 32 (1995) 1355–1389.
[19] R. Holtzman, R. Kastner, On the time domain discrete Green's function at the FDTD grid boundary, IEEE Trans. Antennas Propagat. 49 (7) (2001) 1079–1093.
[20] R. Holtzman, R. Kastner, E. Heyman, R.W. Ziolkowski, Stability analysis of the Green's function method (GFM) used as an ABC for arbitrarily-shaped boundaries, IEEE Trans. Antennas Propagat. 50 (2002) 1017–1029.
[21] S.V. Tsynkov, Numerical solution of problems on unbounded domains, a review, Appl. Numer. Math. 27 (1998) 465–532 (Special issue on absorbing boundary conditions).
[22] D. Givoli, Numerical Methods for Problems in Infinite Domains, Elsevier, Amsterdam, 1992.
[23] F. Ihlenburg, Finite Element Analysis of Acoustic Scattering, Springer, New York, 1998.
[24] W.C. Chew, J.-M. Jin, E. Michielssen, J. Song, Fast and Efficient Algorithms in Computational Electromagnetics, Artech House, Boston, 2001.
[25] V. Rohklin, Rapid solution of integral equations of scattering theory in two dimensions, J. Comput. Phys. 86 (1990) 414–439.
[26] R. Coifman, V. Rokhlin, S. Wandzura, The fast multipole method for the wave equation: a pedestrian prescriptin, IEEE Antennas Propagat. Mag. 35 (1993) 7–12.
[27] C.C. Lu, W.C. Chew, Fast algorithm for solving hybrid integral equations, IEE Proc.-H 140 (1993) 455–460.
[28] N. Lu, J.-M. Jin, Application of the fast multipole method to finite-element boundary-integral solution of scattering problems, IEEE Trans. Antennas Propagat. 44 (1996) 781–786.
[29] B. Dembart, E. Yip, A 3D fast multipole method for electromagnetics with multiple levels, in: 11th Annual Rev. Progress Appl. Computat. Electromag., 1995, pp. 621–628.
[30] J.M. Song, W.C. Chew, Multilevel fast-multipole algorithm for solving combined field integral equations of electromagnetic scattering, Microwave Opt. Technol. Lett. 10 (1) (1995) 14–19.

[31] J.M. Song, C.C. Lu, W.C. Chew, MLFMA for electromagnetic scattering by large complex objects, IEEE Trans. Antennas Propagat. 45 (1997) 1488–1493.
[32] L. Greengard, J. Huang, V. Rokhlin, S. Wandzura, Accelerating fast multipole methods for the Helmholtz equation at low frequencies, Comput. Sci. Engrg. 5 (1998) 32–38.
[33] E. Darve, The fast multipole method I: error analysis and asymptotic complexity, SIAM J. Numer. Anal. 38 (1999) 98–128.
[34] E. Darve, The fast multipole method: numerical implementation, J. Comput. Phys. 160 (2000) 195–240.
[35] A. Boag, U. Shemer, R. Kastner, Fast global radiation boundary conditions based on non-uniform grid approach, URSI North American Radio Science Meeting, Columbus, Ohio, 2003.
[36] A. Boag, A fast iterative physical optics (FIPO) algorithm based on non-uniform polar grid interpolation, Microwave Opt. Technol. Lett. 35 (3) (2002) 240–244.
[37] J. Liu, J.M. Jin, A novel hybridization of higher order finite element and boundary integral methods for electromagnetic scattering and radiation problems, Research Report No. CCEM-15-00 University of Illinois, Urbana, 2000.
[38] D. Jiao, M. Lu, E. Michielssen, J.-M. Jin, A fast time-domain finite element—boundary integral method for electromagnetic analysis, IEEE Trans. Antennas Propagat. 49 (10) (2001) 1453–1461.
[39] A. Boag, U. Shemer, R. Kastner, Hybrid non-uniform grid based fast global boundary conditions for concave scatters, in: Proceedings of the International IEEE Symposium on Antennas and Propagation, Monterey, California, USA, 2004, pp. 627–630.